JOURNAL OF AGRICULTURAL AND FOOD CHEMISTRY

Article

pubs.acs.org/JAFC

Temperature- and Pressure-Dependent Densities, Self-Diffusion Coefficients, and Phase Behavior of Monoacid Saturated Triacylglycerides: Toward Molecular-Level Insights into Processing

Maximilian Greiner, Anthony M. Reilly, and Heiko Briesen*

Chair for Process Systems Engineering, Technische Universität München, Weihenstephaner Steig 23, D-85354 Freising, Germany

ABSTRACT: Using molecular-dynamics (MD) simulations the densities and self-diffusion coefficients of a range of liquid monoacid triacylglycerides (TAGs) have been studied as a function of temperature and, for the first time, pressure. While offset by their ambient properties, the response of the TAGs to temperature and pressure is qualitatively similar. Application of pressure was found to significantly increase densities and reduce diffusion of the TAG molecules, suggesting that it may have as much a role in processing and crystallizing TAGs as supercooling does. A solution of glycerol tripalmitate and glycerol trihexanoate was also studied, showing that application of pressure should lead to a significant decrease in the saturation point of the solution, which is an important consideration for processing TAGs. Different solid/liquid interfaces of glycerol tripalmitate have also been investigated. Although crystal growth could not be observed, dissolution of one interface was seen in the MD simulations. The results suggest that over moderate distances the melting of TAGs may be cooperative in nature, rather than involving dissolution of individual TAG molecules.

KEYWORDS: *triacylglycerides, high-pressure processing, phase diagram, dissolution*

INTRODUCTION

High-pressure treatment of foods has become increasingly important in recent years, as it can be an effective method for inactivation of bacteria with less impact on texture, color, and flavor when compared with thermal processing.[1] One of the major ingredients in many foods are triacylglycerides (TAGs), where three fatty acids are attached to a glycerol backbone via an ester bond. To devise and employ high-pressure processes effectively, a fundamental understanding of the underlying dynamics is needed, such as knowledge of phase-transition diagrams[2,3] or the response of the system to pressure and composition changes.[4]

These types of properties are, in principle, obtainable from molecular-dynamics (MD) simulations. MD simulations have been used a number of times previously to study TAG properties.[5] Sum et al.[6] developed a force field for TAGs derived from an earlier force field for aliphatic chains.[7−9] With this parameter set, the liquid properties of TAGs were explored as a function of temperature, including their tendency to aggregate into bilayers.[6,10]

Formation of crystalline TAGs is of particular relevance to industry as many food stuffs, such as, e.g., chocolate, include solid TAGs. TAGs are known to crystallize in α, β, and β' polymorphs, with β being the most thermodynamically stable.[11] Solidification of fats has also been explored using a lipid-based force field, with crystalline ordering being observed in annealed simulations on the order of 300−700 ns.[12] However, the detailed and routine simulation of nucleation is still very difficult due to the long time scales (relative to the MD time scale) upon which nucleation occurs.

In the present work, we perform MD simulations of liquid TAGs to assess the role of temperature and pressure on their properties with the aim of understanding the interplay between pressure and temperature processing better. In addition, the two possible solid/liquid interfaces of a particular TAG have been studied. While growth of TAGs onto the existing lattice could not be seen, it was possible to simulate dissolution. Dissolution is also an important phenonomena as recrystallization of TAGs is known to occur in foods, possibly mediated by solution or liquid TAG present.[13] In the following section the details of MD simulations and investigated TAGs studied are given.

SIMULATION METHODS

In the present work five monoacid TAG molecules have been studied, namely, glycerol tributyrate (BBB), glycerol trihexanoate (HHH), glycerol trilaurate (LLL), glycerol tripalmitate (PPP), and glycerol tristearate (SSS). For each molecule the force field of Nath et al.[7−9] was used to model the aliphatic chains, while the central glycerol core of the TAG was modeled using the parameters of Sum et al.[6] The various Lennard−Jones nonbonded interactions were determined using the literature self-interaction parameters and the Loretz−Berthelot combination rules.[14]

The Gromacs simulation code (version 4.5.4)[15,16] was used to perform all of the simulations. Long-range electrostatics were treated with the particle-mesh Ewald method.[14] A nonbonded interaction cutoff distance of 1.1 nm was used with a shift to smoothly decrease to a value of zero at 1.4 nm. A time step of 2 fs was used for all MD simulations. For production *NVT* and *NPT* simulations, the temperature was controlled using the Nosé−Hover thermostat.[17,18] The pressure was controlled using an isotropic (for liquids) or anisotropic (for solids and interfaces) Parrinello−Rahman barostat.[19] In some equilibration simulations a Berendsen thermostat or barostat[20] was used to prevent large fluctuations in temperature or pressure when far from equilibrium. The positions and velocities of the

Received: February 7, 2012
Revised: April 2, 2012
Accepted: April 13, 2012
Published: April 14, 2012

atoms were recorded every 2 ps for solid and liquid simulations and every 12 ps for solid/liquid interface simulations.

The initial coordinates for the TAG molecules were obtained from the PRODRG server,[21] and from this simulation cells containing 160 molecules were built. Generating the simulation cells lead to large gaps in the initial configurations, so care was taken in equilibrating the systems with the cell allowed to contract at a particular temperature. Equilibration simulations at other temperatures were performed using this contracted cell as a starting point. A similar procedure was used to generate solutions of PPP and HHH, where 16, 32, and 48 molecules of PPP were inserted into a large simulation boxes and 144, 128, and 112 molecules of HHH were then subsequently added. For studies of solid PPP the β crystal structure was obtained from Langevelde et al.[22] The unit cell was duplicated 10, 4, and 2 times in the x, y, and z directions, respectively, to obtain a supercell suitable for simulation, which contained 160 TAG molecules.

For the liquid systems, the density, self-diffusion coefficient, and other properties were calculated at various pressures and temperatures. Densities were averaged over 6 ns production simulations, while self-diffusion coefficients were calculated from the slope of the mean squared displacements in the linear region between 2 and 4 ns. When calculating volumes and densities for the solid−liquid coexistence calculation of PPP, production simulations were performed for 3 ns with a 2 ns period of equilibration before any subsequent production simulation at a different pressure or temperature.

Two solid/liquid interfaces for PPP were obtained by slicing the PPP unit cell crystal structure along two particular Miller indeces [(001) and $(01\bar{2})$] so that the resulting crystal faces were perpendicular to the z axis. The starting sliced crystal cells both contained 4 molecules. They were replicated 6, 4, and 5 times in the x, y, and z directions, respectively, for the (001) interface and 5, 3, and 8 times, respectively, for the $(01\bar{2})$ interface, making two crystal slabs each with 480 TAG molecules. This operation was performed using the GDIS program.[23] Extending the simulation box in the z direction gave a large gap into which a pre-equilibrated slab of 1520 liquid PPP molecules was inserted. This initial configuration was then subject to energy minimization, followed by an *NVT* simulation where the crystal was constrained while the liquid was heated. Thereafter, the crystal particles were allowed to move in the z direction during an *NPT* simulation at 339 K so as to make the box contract to a more physically reasonable value. A further *NPT* equilibration simulation was then performed prior to any production simulation. The typical length of a production simulation was 70 ns.

In addition to the density and other quantities, the radius of gyration can be used as a measure of whether a TAG molecule is crystalline or not. Rather than considering the distances between all atoms and the center of mass, we define the radius of gyration based on the distances between the central C atom and the end atom of each of the aliphatic chains

$$R_g = \sqrt{\frac{1}{3}\left\langle \sum_{i=1}^{3} r_i^2 \right\rangle} \quad (1)$$

where r_i is the distance between the ith chain terminus and the central C atom. The value of eq 1 is larger in the solid state as the chains are elongated in the crystal structure. In solution they will more likely curl back toward the central atom. In the solid/liquid interface calculation, R_g can be readily calculated as a function of the z coordinate of the simulation cell by dividing the cell into slabs.

RESULTS AND DISCUSSION

Temperature-Dependent Liquid Properties. In Figure 1a the densities of BBB, HHH, LLL, PPP, and SSS are shown as a function of temperature. The temperature dependence of bilayer structures of LLL and SSS has been reported previously using the same force field,[10] while a proper validation of the force field with both experimental and theoretical values at various temperatures has been reported for all of the TAGs

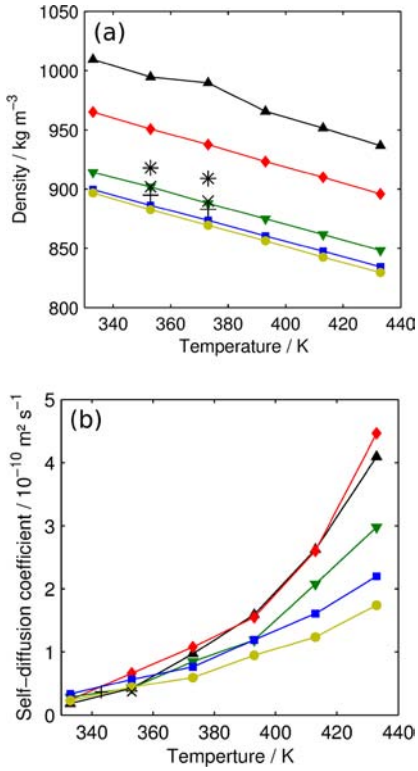

Figure 1. Plots of the temperature dependence of (a) the density and (b) the self-diffusion coefficient for the TAGs BBB (triangle pointing upward), HHH (diamond), LLL (triangle pointing downward), PPP (square), and SSS (circle) with reference values given for LLL[6] (*), PPP[6,12] (×), and SSS[6,24] (+).

apart from BBB and HHH.[6] Our results are in reasonable agreement with previous calculations with the density of LLL at a temperature of 353 K being simulated as 902 kg m^{-3}, while reference simulation values were 918 kg m^{-3}, and experimental values were 882 kg m^{-3}.[6] The trend also shows good agreement with reference values. Therefore, we assume a proper implementation of the force field, whose detailed validation may be found in the paper by Sum et al.[6] Despite the large difference in the chain lengths (BBB has four carbon atoms in each chain, while SSS has 18 carbon atoms in each chain), all of the TAGs exhibit the same decrease in density with temperature, with virtually the same slope for each molecule. As has been observed before the density is higher for the smaller TAG molecules. It is noticeable here though, comparing a wider range of TAGs, that the effect of increasing the chain length is far greater for the smaller molecules. This is intuitive if we consider that for the smaller chains the interactions of the polar core of the molecules will have a dominant role in controlling the density; with each additional pair of carbon atoms this interaction is reduced further and further, so that for the larger chains adding carbons has far less influence.

The self-diffusion coefficients have also been determined as a function of temperature and are shown in Figure 1b along with reference values.[12,24] As we might expect, the general trend is an increase of the diffusion with temperature, with each TAG molecule following Arrhenius dependence. At low temperatures the TAGs all have very similar self-diffusion coefficients, and it is only at high temperatures that large differences appear. The TAGs with longer chains have smaller self-diffusion coefficients, which likely arises from the great chance of chains becoming

entangled when they are longer. Other systems that would be expected to behave similarly, namely, fatty acids and aliphatic chains, are reported to show the same trends.[25,26] Of the two smaller chains, BBB and HHH, HHH has the higher self-diffusion coefficient. This may arise from interactions between the polar core of the small TAG molecule having a more dominate effect on its dynamics. In addition, entanglement is very unlikely with such short chains.

Pressure-Dependent Liquid Properties. The force field of Sum et al.[6] has been shown in the past and by the results of the previous section to produce both qualitatively and quantitatively good agreement with experimental data. However, it has not been used previously for the study of pressure-dependent properties. In Figure 2a the density is

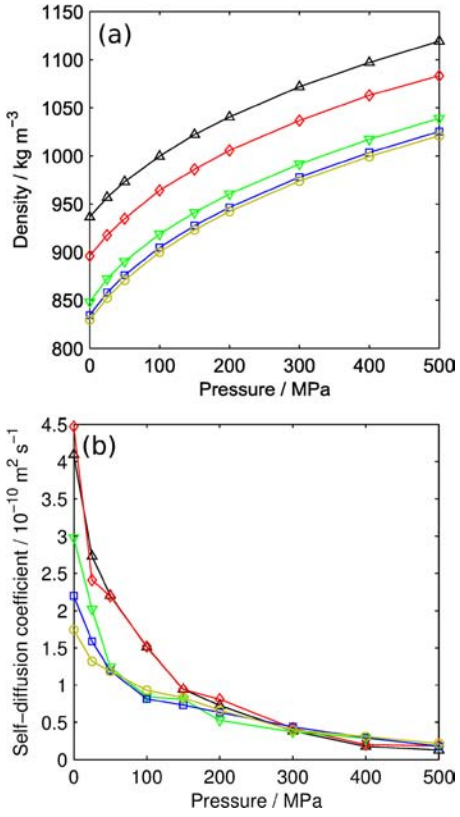

Figure 2. Plots of the pressure dependence of (a) the density and (b) the self-diffusion coefficient for the TAGs BBB (triangle pointing upward), HHH (diamond), LLL (triangle pointing downward), PPP (square), and SSS (circle), all calculated at 433 K.

plotted for the monoacid TAGs as a function of pressure. Comparing the LLL values at 353 K in the range of 0.1−150 MPa to those reported in the literature previously[27] in Table 1, it can be seen that the relative change in the density with pressure is only slightly underestimated by 0.6−1.4% with the absolute values being off by 9−21 kg m^{-3}. Such minor deviations from the experimental values suggest that the Sum et al.[6] force field is also suitable for exploring pressure-controlled properties of monoacid TAGs. As experimental treatments can reach pressures in excess of 600 MPa,[1] it is worth considering the effect of such large pressures on TAGs.

It can be seen from Figure 2a that pressure affects each of the TAGs to the same extent, irrespective of their size. As pressure is expected to drive a liquid toward solidification, for these simulations a temperature of 433 K was chosen. This choice

Table 1. Comparison of Simulated Densities of LLL under High Pressures to Reference Values at a Temperature of 353 K

	simulation		reference[a]	
pressure/MPa	density/kg m^{-3}	relative change/%	density/kg m^{-3}	relative change/%
0.1	914		893	
50	933	2.1	924	3.5
100	956	4.6	943	5.6
150	977	6.9	960	7.5

[a]Reference 27.

was made as to explore the pressure dependence of a liquid at high pressures before reaching phase equilibrium. The effect of pressure is greater at small pressures, presumably as gaps in the liquid are excluded before becoming more linear at high pressures (>250 MPa). Pressure also has a big impact on the self-diffusion coefficients of the TAG molecules as shown in Figure 2b. All of the TAGs experience a significant drop in their thermal motion and diffusion. From 150 MPa their self-diffusion coefficients are all very similar and decrease far less with increasing pressure.

Comparison of Temperature- and Pressure-Dependent Liquid Properties. Figures 1 and 2 show that pressure and temperature can both have a big impact on the properties of TAGs. To compare their influence we considered the effects of cooling and pressurizing on LLL, starting from its melting point at ambient pressure, which is shown in Figure 3. Both

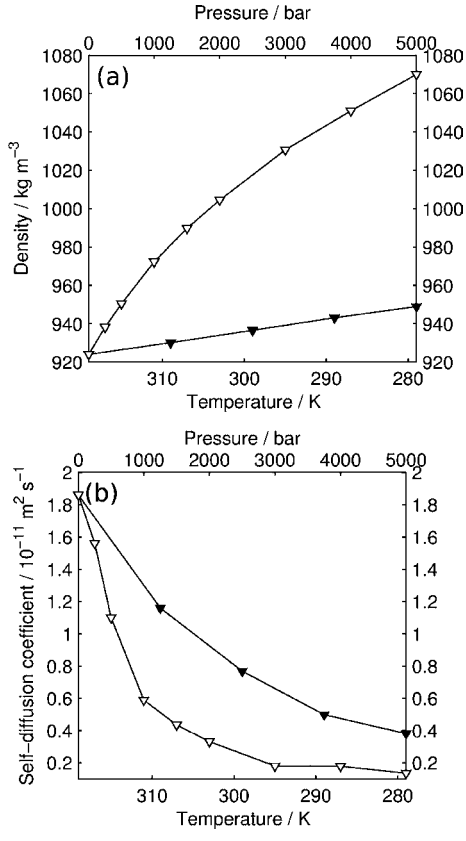

Figure 3. Plots of (a) the density and (b) the self-diffusion coefficient as a function of temperature at 0.1 MPa (closed indicators) and pressure at 319 K (open indicators) for LLL. Note that the temperature scale is reversed.

dx.doi.org/10.1021/jf3004898 | J. Agric. Food Chem. 2012, 60, 5243−5249

cooling and pressurizing will make the liquid metastable,[2] which ultimately should lead to nucleation. Nucleation is not observed in our simulations as the time scale for nucleation is at least 2 orders of magnitude longer than the simulation times used here.[12] However, the effect of pressure on the density and self-diffusion coefficient can be readily determined. Figure 3a shows that the density increases much more in the range of 0.1−500 MPa than in the range from 319 to 280 K, and to obtain the same effect with supercooling would require very low temperatures (<200 K). Similar behavior is seen for the self-diffusion coefficients (Figure 3b), where pressure reduces the self-diffusion coefficient more than temperature, although above a pressure of 300 MPa only little change is observed.

These results, in part, shed some light on the possible mechanism for nucleation. The first step in TAG nucleation from the melt is thought to be stacking of lamella,[11] after which the subcells begin to pack.[28] Application of pressure is known to reduce the induction time for nucleation, even above pressures of 300 MPa.[2] As Figure 3b shows little change in the diffusion of the TAGs molecules above 300 MPa, it seems likely that the role of pressure in inducing crystallization is not just to restrict thermal motion. It is possible that the increased density at higher pressure increases the interactions between TAGs, allowing for faster ordering of the TAG molecules into lamella. However, too high a density (and hence pressure) might make formation of a well-ordered structure difficult, leading to an amorphous solid with potentially poor physical characteristics from the perspective of food science. While further work on the influence of pressure on nucleation is needed, it is clear that MD simulations can give useful insights into developing processing methods, and the results of the present work suggest that any detailed experimental study of one monoacid TAG in the liquid state will be transferable to the other TAGs.

PPP Phase-Transition Diagram Estimation. Presently, only a few phase-transition diagrams have been reported for single-component TAGs.[29] The solid−liquid coexistence curve would be of particular use in understanding the interplay between pressure and temperature for TAGs. There are a variety of ways in which computer-simulation methods can be used to calculate solid−liquid coexistence curves. The Gibbs ensemble scheme uses two simulations of the different phases using exchange of particles between the simulations cells to equalize the chemical potential.[30] Insertion of particles of the size and shape of fat molecules makes such an approach computationally demanding.[31]

Instead, here we employ a simple Gibbs−Duhem integration scheme.[32,33] This involves simulating both phases at a known point on the phase-transition diagram. A small variation in the temperature is made, and the pressure is adjusted to make the chemical potentials of the two phases equal. In this work the new pressure is estimated using simple integration of the Clausius−Clapeyron relation

$$\frac{\mathrm{d}p}{\mathrm{d}T} = \frac{\Delta H_\mathrm{f}}{T\Delta V} \tag{2}$$

where $(\mathrm{d}p)/(\mathrm{d}T)$ gives the slope in a pT phase transition diagram, ΔH_f is the molar enthalpy of fusion, which for PPP is available in the literature,[34] T is the temperature, and ΔV is the difference in molar volume between the crystal and the liquid state, calculated as[29]

$$\Delta V = M\frac{\rho_\mathrm{s} - \rho_\mathrm{l}}{\rho_\mathrm{s}\rho_\mathrm{l}} \tag{3}$$

where M is the molar mass, ρ_s is the mass density for the solid, and ρ_l is the mass density for the liquid phase. Hence, knowing the value of ΔV at a certain T and P an estimate for a linear portion of the solid−liquid coexistence curve can be made. This approach has been used to calculate the coexistence curve for the β form of PPP, starting from its known melting point at ambient pressure, with the result shown in Figure 4, along with

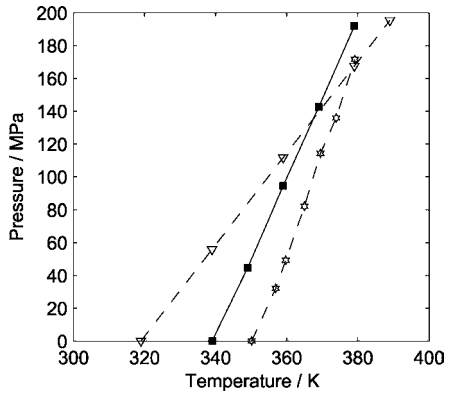

Figure 4. Plot of the calculated solid−liquid coexistence line for PPP (filled squares) with an experimental line for AAA[35] (stars) and a theoretical estimate for LLL (open triangles) based on Lee et al.

an experimental curve for triarachidin (AAA; with 20 C atoms in the ailiphatic chain),[35] which was the only experimental curve for an unsaturated monoacid TAG readily available in the literature. An estimate for the coexistence curve for LLL has been made using the Clausius−Clapeyron relation and a single value for ΔV determined previously by Lee et al.[29] The trends for AAA and PPP are in reasonable agreement, and given the smooth and quantitatively similar behavior for the liquid properties as a function of temperature and pressure, it is not surprising that they should have similar slopes. Estimation for the phase-transition diagram of LLL, however, indicates a larger volume change for smaller chains. As the precise crystal coordinates for the other TAGs are either unknown or hard to obtain, we have not been able to calculate the coexistence line for them. However, the encouraging qualitative agreement with AAA is an incentive for future experimental and computational work on TAG phase-transition diagrams.

Volume Change upon Dissolution for Binary Mixtures. In the previous sections we discussed the influence of temperature and pressure on pure liquids of TAGs. In many instances, TAGs are not crystallized from the melt but from a solution comprised of different TAGs.[2,3] In solution, crystallization and nucleation of a solute typically occurs above a certain saturated concentration. Addition of extra solute above this saturation point can lead to crystal growth. Temperature and pressure can be used to alter the saturation point itself. The effect of pressure on the saturation mole fraction is given by[36]

$$\left(\frac{\partial \ln(x_\mathrm{sat})}{\partial p}\right)_T = -\frac{\Delta V_\mathrm{diss}}{RT} \tag{4}$$

where x_sat is the equilibrium solute mole fraction and ΔV_diss is the molar volume change associated with dissolution. If ΔV_diss is positive, application of pressure will shift the equilibrium toward the solid to reduce the volume of the system. While calculating the value of x_sat is quite difficult without some form

of chemical-potential calculation, the value of ΔV_{diss} can be readily obtained from the densities of the crystal and solution states using an expression of the form of eq 3. This has been used to calculate ΔV_{diss} for solutions of PPP and HHH. For a mole fraction of $x_{PPP} = 0.1$, $\Delta V_{diss} = 113.2$ cm^3 mol^{-1}. For ideal solutions, ΔV_{diss} should be independent of x_{PPP}, but not surprisingly, for such bulky molecules, ΔV_{diss} does vary with x_{PPP}, decreasing to a value of 97.9 cm^3 mol^{-1} for $x_{PPP} = 0.3$. Typically, for a small rigid molecule ΔV_{diss} will be quite small. Although for organic molecules without ionic interactions (e.g., naphthalene) in water[36] and ionic molecules in organic solvents[37] it can be large. The large values found here suggest yet again that pressure can have an important role in processing and crystallizing TAGs whether from the melt or from solution.

In previous experimental studies of nucleation and crystal growth of LLL from a solution of glycerol trioleate (OOO) it was found that no growth of LLL could be induced below $x_{LLL} = 0.2$.[2] The results here for PPP and HHH would suggest that as the concentration decreases, application of pressure will shift the saturated concentration to lower values. However, there are many aspects to the use of pressure in inducing growth and too high a pressure, much like too much supercooling, has the potential to freeze molecules in place, preventing coordinated assembly of molecules required for crystallization. In the case of OOO and LLL, it may also be the case that the saturation point is greater than $x_{LLL} = 0.2$, even with a reduction induced by application of pressure.

Solid/Liquid Interface Dynamics. Having discussed the influence of pressure and temperature on properties of liquid TAGs, we now attempt to shed some light on the molecular-level processes involved in crystal growth. Nucleation of TAGs has been studied previously[12] and necessitated annealing and simulation times in excess of 300 ns. Instead, here we have chosen to study the solid/liquid TAG interfaces, taking the known crystal structure of PPP to form interfaces between the (001) and the $(01\bar{2})$ faces and a liquid slab (see Figure 5). In the (001) face the TAG molecules are aligned perpendicular to the plane of the face, making integration into the crystal very difficult. In the $(01\bar{2})$ case, the TAG molecules are more parallel to the interface, although they have a small angle of tilt with respect to the face. This leaves a slight overhang on the surface, which in our simulations quickly disappears, leading to a reconstructed surface where the TAG molecules are exactly parallel to the interface. This makes the two cases the limits of the TAG alignment with respect to the interface. The equilibrated (001) interface also shows an imperfect structure in the lattice, where planes of TAGs have slipped relative to others. While both cases may well be a result of the small size of the crystalline slab and the equilibration procedure, it is also an indication that on the scale of 5 or 6 unit cells TAG molecules can readily undergo cooperative behavior.

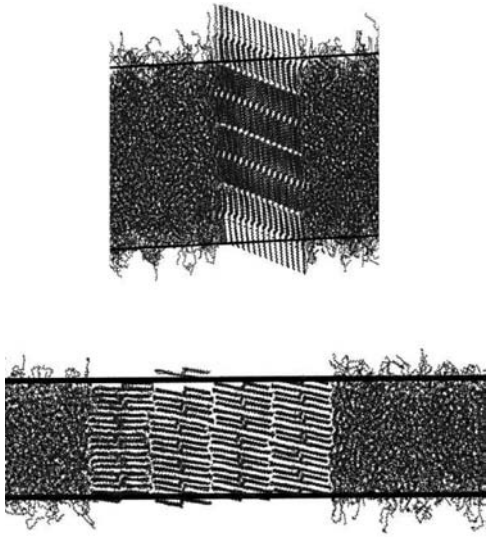

Figure 5. Plot of the equilibrated starting configurations of solid/liquid PPP interfaces at a temperature of 359 K for the reconstructed $(01\bar{2})$ face (top) and the (011) face (bottom).

Attempts were made to simulate growth from the melt for the two TAG interfaces. Solidification due to the impact of pressure would be of great interest: first, to investigate the polymorph favored by pressure-induced solidification and, second, to compare the mechanisms between inducing supersaturation by a decrease of temperature and an increase of pressure. The melting point of PPP is 339 K at 0.1 MPa.[34] However, in simulations up to 270 ns in length no crystal growth could be seen for either face, even when simulating at 309 K and 400 MPa. Simulations with intermediate supercooling and pressurizing also show no growth. The (001) face is the largest in experimental crystal morphologies[38] and therefore is likely to be the slowest growing. From a molecular viewpoint this makes considerable sense given the need for molecules to align perpendicular to the interface. For the reconstructed $(01\bar{2})$ interface we would expect growth to be much faster, but this may still be beyond the time scale of the MD simulations. While some supercooling and pressurizing will make growth faster, too much may restrict the movement of the liquid TAGs, hindering their assembly on the surface.

While growth was not observable on the MD time scale, dissolution of the TAG crystals was seen for the reconstructed $(01\bar{2})$ interface. In a 70 ns simulation at 359 K and 0.1 MPa, the crystal slab melted appreciably while the (001) face showed no dissolution. This can be easily seen in the plots of the radius of gyration as a function of the z coordinate of the simulation cells (Figure 6). The crystal slab is represented by the area of high radius of gyration. The lattice planes in the (001) simulation can be seen in the regions where there are no TAG atoms present at all and the lines of Figure 6 are broken. No change in structure occurs during the 70 ns simulation, even though the system is 20 K above the known melting point of PPP. In contrast, the $(01\bar{2})$ surface shows dissolution within the first 30 ns. As time proceeds the high R_g region gets smaller, and by the end of the 70 ns the crystal slab has reduced in size by approximately 50%. It is worth noting that rather than layers of the crystal dissolving without any impact on the remaining crystal slab the value of R_g decreases with time as well. In fact, the decrease in the value of R_g is much more noticeable over the range of 0−50 ns than the decrease in the width of the crystal slab. This suggests that the entire slab undergoes changes, becoming less ordered up until a point at which rapid dissolution can occur. The width of the slab is at least 5−6 times the LJ cutoff distance, suggesting that while finite-size effects may play some role, dissolution of TAGs may involve cooperative behavior of the TAG molecules.

In summary, MD simulations have been performed using a literature force field for TAGs[6] to investigate a number of different properties of monoacid TAGs. The densities and self-diffusion coefficients of liquid TAGs with aliphatic chain lengths ranging from 4 to 18 C atoms have been studied as a

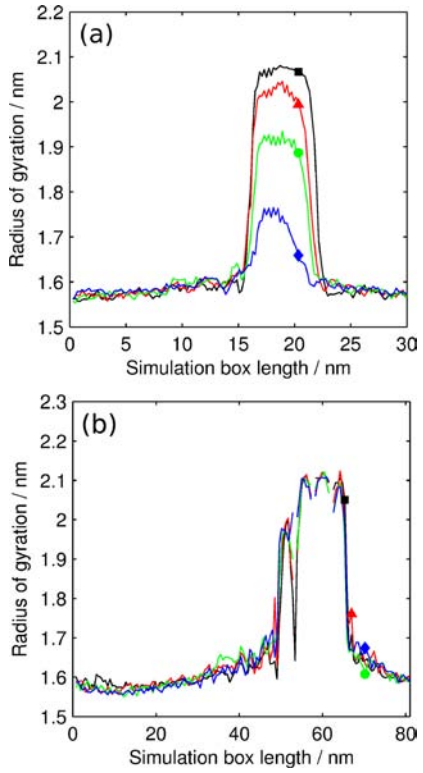

Figure 6. Plots of the radius of gyration for PPP solid/liquid interfaces with (a) the reconstructed $(01\bar{2})$ and (b) the (001) face, both simulated for 70 ns at a temperature of 359 K. Time averages are given for 0−17.5 (square), 17.5−35 (triangle), 35−52.5 (circle), and 52.5−70 ns (diamond).

function of temperature and pressure. All of the TAGs show similar behavior, with pressurizing and cooling leading to similar significant increases in densities and decreases in self-diffusion coefficients.

Taking the example of PPP, selected aspects of the crystallization of TAG molecules have been explored. The PPP solid−liquid coexistence line has been estimated using a simple variant of the Gibbs−Duhem integration scheme.[32,33] Experimental coexistence curves for TAGs are hard to obtain, and none at present exists for PPP. The qualitative agreement between the simulated PPP curve and an experimental curve for AAA is encouraging. In addition, solutions of HHH and PPP were simulated to understand the volume change associated with dissolution. This value is directly related to the influence of pressure on the saturation point of the solution. It was found to be very large, greater than 100 $cm^3\ mol^{-1}$ when the PPP mole fraction was 0.2 or lower. This result and the studies of the liquid TAG properties suggest that pressure can have a big role in processing TAGs, particularly in pressure-induced crystallization, which has already been observed experimentally.[2,3]

Finally, we also performed simulations of the PPP solid/liquid interface, taking the (001) and $(01\bar{2})$ faces as limits, as in the latter the TAG molecules are parallel to the plane of the interface and in the former they are perpendicular to the interface. For both interfaces no ordering or attachment of TAG molecules could be seen in 270 ns long simulations, even with supercooling and pressurizing. Dissolution of the $(01\bar{2})$ solid/liquid interface could be simulated. The crystal slab melted in a two-stage process, where order was lost throughout the slab, followed by fast dissolution from the edges of the slab. While finite-size effects may play a role, here it is an indication that cooperative behavior of TAGs is possible over moderate distances.

AUTHOR INFORMATION

Corresponding Author

*E-mail: heiko.briesen@mytum.de.

Funding

This work was supported by the Deutsche Forschungsgemeinschaft (DFG) through grant BR 2035/4-1.

Notes

The authors declare no competing financial interest.

ACKNOWLEDGMENTS

This work made use of the computer resources provided by the Leibniz Supercomputing Centre. The ScalaLife Competence Center (http://www.scalalife.eu/) is also acknowledged for assistance with computing resources and the Gromacs code. M.G. gratefully acknowledges the support by the Faculty Graduate Center Weihenstephan of TUM Graduate School at Technische Universität München, Germany.

REFERENCES

(1) Torres, J. A.; Velazquez, G. Commercial opportunities and research challenges in the high pressure processing of foods. *J. Food Eng.* **2005**, *67*, 95−112.

(2) Ferstl, P.; Gillig, S.; Kaufmann, C.; Dürr, C.; Eder, C.; Wierschem, A.; Ruß, W. Pressure-induced phase transitions in triacylglycerides. *Ann. N.Y. Acad. Sci.* **2010**, *1189*, 62−67.

(3) Ferstl, P.; Eder, C.; Ruß, W.; Wierschem, A. Pressure-induced crystallization of triacylglycerides. *High Pressure Res.* **2011**, *31*, 339−349.

(4) LeBail, A.; Boillereaux, L.; A., D.; Hayert, M.; Lucas, T.; Monteau, J. Phase transition in foods: effect of pressure and methods to assess or control phase transition. *Innov. Food Sci. Emerg. Technol.* **2003**, *4*, 15−24.

(5) Yan, Z. Y.; Huhn, S. D.; Klemann, L. P.; Otterburn, M. S. Molecular modeling studies of triacylglycerols. *J. Agric. Food Chem.* **1994**, *42*, 447−452.

(6) Sum, A. K.; Biddy, M. J.; de Pablo, J. J.; Tupy, M. J. Predictive molecular model for the thermodynamic and transport properties of triacylglycerols. *J. Phys. Chem. B* **2003**, *107*, 14443−14451.

(7) Nath, S. K.; Escobedo, F. A.; de Pablo, J. J. On the simulation of vapor-liquid equilibria for alkanes. *J. Chem. Phys.* **1998**, *108*, 9905−9911.

(8) Nath, S. K.; Khare, R. New forcefield parameters for branched hydrocarbons. *J. Chem. Phys.* **2001**, *115*, 10837−10844.

(9) Nath, S. K.; Banaszak, B. J.; de Pablo, J. J. A new united atom force field for α-olefins. *J. Chem. Phys.* **2001**, *114*, 3612−3616.

(10) Hsu, W. D.; Violi, A. Order-disorder phase transformation of triacylglycerols: effect of the structure of the aliphatic chains. *J. Phys. Chem. B* **2009**, *113*, 887−893.

(11) Himawan, C.; Starov, V. M.; Stapley, A. G. F. Thermodynamic and kinetic aspects of fat crystallization. *Adv. Colloid Interface Sci.* **2006**, *122*, 3−33.

(12) Hall, A.; Repakova, J.; Vattulainen, I. Modeling of the triglyceride-rich core in lipoprotein particles. *J. Phys. Chem. B* **2008**, *112*, 13772−13782.

(13) Hernquist, L. In *Crystallization and Polymorphism of Fats and Fatty Acids*; Garti, N., Sato, K., Eds.; Marcel Dekker Inc., New York, 2001; Chapter Crystal structures of fats and fatty acids, pp 97−138.

(14) Allen, M. P.; Tildesley, D. J. In *Computer Simulation of Liquids*; Oxford University Press Inc.: New York, 1989.

(15) Van der Spoel, D.; Lindahl, E.; Hess, B.; Groenhof, G.; Mark, A. E.; Berendsen, H. J. C. GROMACS: Fast, flexible, and free. *J. Comput. Chem.* **2005**, *26*, 1701−1718.
(16) Hess, B.; Kutzner, C.; van der Spoel, D.; Lindahl, E. GROMACS 4: Algorithms for highly efficient, load-balanced, and scalable molecular simulation. *J. Chem. Theory Comput.* **2008**, *4*, 435−447.
(17) Nosé, S. A unified formulation of the constant temperature molecular dynamics methods. *J. Chem. Phys.* **1984**, *81*, 511−519.
(18) Hoover, W. G. Canonical dynamics: Equilibrium phase-space distributions. *Phys. Rev. A* **1985**, *31*, 1695−1697.
(19) Parrinello, M.; Rahman, A. Polymorphic transitions in single-crystals - a new molecular-dynamics method. *J. Appl. Phys.* **1981**, *52*, 7182−7190.
(20) Berendsen, H. J. C.; Postma, J. P. M; van Gunsteren, W. F.; Dinola, A.; Haak, J. R. Molecular dynamics with coupling to an external bath. *J. Chem. Phys.* **1984**, *81*, 3684−3690.
(21) Schuttelkopf, A. W.; van Aalten, D. M. F. *PRODRG*: a tool for high-throughput crystallography of protein-ligand complexes. *Acta Crystallogr., Sect. D: Biol. Crystallogr.* **2004**, *60*, 1355−1363.
(22) van Langevelde, A.; van Malssen, K.; Sonneveld, E.; Peschar, R.; Schenk, H. Crystal packing of a homologous series *β'*-stable triacylglycerols. *J. Am. Oil Chem. Soc.* **1999**, *76*, 603−609.
(23) Fleming, S.; Rohl, A. GDIS: a visualization program for molecular and periodic systems. *Z. Kristallogr.* **2005**, *220*, 580−584.
(24) Callaghan, P. T.; Jolley, K. W. Translational Motion In the Liquid Phases of Tristearin, Triolein and Trilinolein. *Chem. Phys. Lipids* **1980**, *27*, 49−56.
(25) Iwahashi, M.; Y., K.; Minami, H.; Matsuzawa, H.; Suzuki, M.; Y., O. Molecular behaviors of *n*-fatty acids in liquid state. *J. Oleo Sci.* **2002**, *51*, 157−164.
(26) Harmandaris, V. A.; Doxastakis, M.; Mavrantzas, V. G.; Theodorou, D. N. Detailed molecular dynamics simulation of the self-diffusion of *n*-alkane and *cis*-1,4 polyisoprene oligomer melts. *J. Chem. Phys.* **2002**, *116*, 436−446.
(27) Acosta, G. M.; Smith, R. L.; Arai, K. High-pressure *PVT* behavior of natural fats and oils, trilaurin, triolein, and *n*-tridecane from 303 K to 353 K from atmospheric pressure to 150 MPa. *J. Chem. Eng. Data* **1996**, *41*, 961−969.
(28) Sato, K. Solidification and phase transformation behaviour of food fats - a review. *Fett/Lipid* **1999**, *101*, 467−474.
(29) Lee, Y. L.; Ristic, R. I.; DeMatos, L. L.; Martin, C. M. Crystallisation pathways of polymorphic triacylglycerols induced by mechanical energy. *J. Phys.: Conf. Ser.* **2010**, *247*, 1−16.
(30) Panagiotopoulos, A. Z. Direct determination of phase coexistence properties of fluids by Monte Carlo simulation in a new ensemble. *Mol. Phys.* **1987**, *61*, 813−826.
(31) Ouyang, W. Z.; Lu, Z. Y.; Sun, Z. Y.; An, L. J. Molecular dynamics study on the phase diagrams of linear and branched chain molecules. *Chem. Phys.* **2008**, *344*, 52−60.
(32) Kofke, D. A. Gibbs-Duhem integration: a new method for direct evaluation of phase coexistence by molecular simulation. *Mol. Phys.* **1993**, *78*, 1331−1336.
(33) Kofke, D. A. Direct evaluation of phase coexistence by molecular simulation via integration along the saturation line. *J. Chem. Phys.* **1993**, *98*, 4149−4162.
(34) Hagemann, J. W. In *Crystallization and Polymorphism of Fats and Fatty Acids*; Garti, N., Sato, K., Eds.; Marcel Dekker Inc.: New York, 2001; Chapter Thermal behavior and polymorphism of acylglycerides, pp 9−96.
(35) Masberg, S. Differentialkalorimetrie (DSC) und Differentialthermoanalyse (DTA) bei hohen Drücken: Untersuchungen zum Phasenverhalten ausgewählter Triacylglycerine, Flüssigkristalle und Anthrachinonfarbstoffe bis 200 MPa. Ph.D. thesis, Ruhr-Universität Bochum, Fakultät für Chemie und Biochemie, 1999.
(36) Sawamura, S.; Tsuchiya, M.; Ishigami, T.; Taniguchi, Y.; Suzuki, K. Effect of pressure on the solubility of naphthalene in water at 25 °C. *J. Solut. Chem.* **1993**, *22*, 727−732.
(37) Doane, E. P.; Drickamer, H. G. The effect of pressure on the solubility of solids in non-polar liquids. *J. Phys. Chem.* **1955**, *59*, 454−457.
(38) Hollander, F. F. A.; Plomp, M.; van de Streek, J.; van Enckevort, W. J. P. A two-dimensional Hartman-Perdok analysis of polymorphic fat surfaces observed with atomic force microscopy. *Surf. Sci.* **2001**, *471*, 101−113.